Investigations on Chemical, Thermal Decomposition Behavior, Kinetics, Reaction Mechanism and Thermodynamic Properties of Aged TATB

Arjun Singh,[*] **Gurvinder Kaur, Chinmay Sarkar, Niladri Mukherjee**

Terminal Ballistics Research Laboratory, Explosive Group, Sector 30, Chandigarh, India
[*]*E-mail: arjunsngh@yahoo.com*

Abstract: 1,3,5-triamino-2,4,6-trinitrobenzene (TATB) is a kind of insensitive high explosive that can be used as an energetic material in nuclear weapon and space applications. In this work, we have studied the effect of aging on the properties of TATB from a 20 year old lot that had been in direct contact with casing and natural environment conditions. The kinetics was studied using the temperature at the maximum reaction rate (peak) and isoconversional methods from TGA and DTA data obtained at five heating rates under a nitrogen atmosphere. The properties investigated for thermal stability indicate that there is no change in the properties during prolonged exposure in natural environment conditions. The activation energy calculated by the Kissinger method was 179.9 kJ·mol^{-1} by DTG and the 176.9 kJ·mol^{-1} by DTA. The experimental results of kinetic analysis obtained by isoconversional methods are in good agreement and very close to each other. In the analysis of reaction mechanisms, the reaction models could be probably best described by a surface contraction mechanism using the Coats-Redfern and Criado methods. The thermodynamic parameters such as Gibbs free energy, enthalpy and entropy of activation were also investigated. The self-accelerating decomposition temperature (T_{SADT}) and critical temperature for thermal explosion (T_b) were also calculated.

Keywords: 1,3,5-triamino-2,4,6-trinitrobenzene, thermal decomposition, kinetics, thermodynamics

1   Introduction

1,3,5-triamino-2,4,6-trinitrobenzene (TATB) is well-known insensitive high explosive material which contains a large amount of energy that can be released upon an external stimulus. It is a reasonably powerful high explosive with outstanding properties including high melting point, high thermal stability and insensitivity in terms of impact, friction, and shock. Its insensitivity is considerably greater than that of other known explosives with a similar energy content [1] and is the explosive of preference in military and civil applications [2, 3] where the extreme safety parameters in terms of shock, vibration, fire or impact are required. It is also used as an explosive ingredient for boosters or main explosive formulations in modern nuclear warheads because of its resistance to heat and physical shock. Some TATB-based formulations such as PBX-9502 (95% TATB and 5% Kel-F 800), LX-17 (92.5% TATB and 7.5% Kel-F 800) and PBX-9503 (80% TATB, 15% HMX and 5% Kel-F 800) have been prepared for space and military applications [4, 5].

Most high explosives are organic in nature and have a tendency to undergo slow decomposition during storage under natural environment conditions. The decomposition process degrades the stability of the explosive, thereby resulting in reduced performance and service life. Therefore, the decomposition chemistry is introduced on demand and not accidently in a response to unintended perturbation [6, 7]. It is reported that the properties of TATB are changed upon exposure to a radiation stimulus due to chemical decomposition [8-10]. During the decomposition process, the colour of TATB changes from yellow (for a freshly prepared sample) to green. Increasing the radiation dose prolongs the effects on the bulk properties of TATB. Some theoretical and experimental studies [11, 12] have been undertaken to investigate the effect of radiation on the mechanical and chemical properties of TATB bonded with polymeric binders. TATB may expose with penetrating radiation in the stockpile environment and this may cause the aging signature that is readily manifested with consequences for the lifetime service.

Countries that make nuclear bombs and cruise missile warheads store large quantities of TATB in magazines. The effects of long-term storage of this explosive in natural environment conditions have not been completely investigated due to scarce access to aged material. Due to its high sensitivity for penetrating radiation, we propose to investigate the effect of aging on the properties of TATB from a 20 year old lot stored in a casing under natural environment conditions and to determine whether this material could be used for further military applications or should be destroyed.

This paper presents the result of investigations of the change in thermal decomposition behaviour and thermodynamic properties of aged TATB by means of various analytical techniques. The kinetic analysis was performed by applying peak temperature at the maximum decomposition reaction rate (peak) and the isoconversional (model-free) methods. The self-accelerating decomposition temperature (T_{SADT}) and critical temperature of thermal explosion (T_b) were also investigated and are discussed.

2   Experimental

2.1 Materials

TATB was synthesized in-house by amination of 1,3,5-trichloro-2,4,6-trinitrobenzene in toluene with anhydrous ammonia by the Benziger route, resulting in the formation of crude TATB with chloride impurity. This chloride impurity was removed by boiling the crude TATB in hot water because NH_4Cl has high solubility in water. It was then stored for 20 years in a magazine. During this time, the material was in direct with a casing material and under normal stockpile environmental conditions. Temperature generally varied annually in the range of 4 °C to 47 °C and humidity between 40-95% r.h.

2.2 Characterization of TATB

Particle density was estimated by measurement of the mass per unit volume. The volume of polymeric materials was determined by using a ultra-fine gas pycnometer (manufactured and supplied by M/s Quantachrome). This is based on the Archimedes' principle of fluid displacement and the Boyle's law. In this experiment, helium gas was used as the displacement fluid because of its small molecular size (0.49 Å).

Mass loss measurements were carried out using a Simultaneous Thermal Analyzer (model STA 851^e) as manufactured and supplied by Mettler Toledo Switzerland. Thermogravimetry (TG) was performed from room temperature up to 600 °C at heating rates of 5 °C·min^{-1}, 10 °C·min^{-1}, 20 °C·min^{-1}, 30 °C·min^{-1} and 40 °C·min^{-1} under a nitrogen atmosphere using 5.5 ±0.5 mg samples in an open pan alumina crucible. The flow rate of nitrogen gas was kept constant at 30 cm^3·min^{-1}. DTA analysis was performed using sealed standard 40 μL aluminum crucibles containing 4.0 ±0.5 mg samples. The samples were heated from 25 °C up to 600 °C at a heating rate of 10 °C·min^{-1} under a nitrogen atmosphere.

A Fourier transform infrared spectrophotometer (FTIR Nicolet Avtar 360

model) was used to identify the chemical structure of the aged TATB. An FTIR spectrum was obtained from samples which were ground with KBr and then pressed into pellet form. The spectrum was recorded from 4000 cm^{-1} to 400 cm^{-1}. The surface morphology was studied using a Carl-Zeiss EVO 5 Scanning Electron Microscope (SEM). The samples were sputter coated with gold before analysis.

2.3 Theoretical approach for kinetic study

Solid-state kinetics is generally studied by means of thermogravimetric analysis [13-15] which measures change in mass when material is subjected to heat or held at a constant temperature. For the thermal decomposition, the rate of reaction is described by two functions: the rate constant (k) and the extent of the conversion (α):

$$\frac{d\alpha}{dt} = k f(\alpha) \tag{1}$$

where k is the reaction rate constant, α is the extent of conversion, and $f(\alpha)$ is the differential form of the kinetic model, which is function of α. The temperature dependence of the rate constant k is usually given by the Arrhenius equation:

$$k = Ae^{-\frac{E_a}{RT}} \tag{2}$$

where A is the pre-exponential factor, E_a is the activation energy, T is the absolute temperature and R is the gas constant (8.314 J·mol^{-1}·K^{-1}). For non-isothermal TGA, α at any time t is given by Equation 3:

$$\alpha = \frac{m_o - m_t}{m_o - m_\infty} \tag{3}$$

where m_0 is the initial mass, m_t is the mass at time t, and m_∞ is the final mass of the sample. The rate constant k is usually given by the Arrhenius equation by using a wide variety of reaction models $f(\alpha)$. Comparing Equations 1 and 2 the following Equation 4 is obtained as:

$$\frac{d\alpha}{dt} = Ae^{-\frac{E_a}{RT}} f(\alpha) \tag{4}$$

Equation 4 is the fundamental expression of analytical methods used for determining kinetic parameters on the basis of TGA data.

2.3.1 The Flynn-Wall-Ozawa (FWO) method

Flynn, Wall [16] and Ozawa [17] proposed a method for calculating kinetic parameters using Doyle's approximation of a temperature integral. It is based on the assumption that thereaction rate depends on the temperature at a constant conversion. The FWO equation describes a simple relationship of activation energy, heating rate and temperature as follows:

$$log(\phi) = log\frac{A_\alpha E_{a\alpha}}{g(\alpha)R} - 2.315 - 0.457\frac{E_{a\alpha}}{RT_\alpha} \tag{5}$$

where T_α is the temperature (K) at constant conversion, ϕ is the heating rate and $E_{a\alpha}$ is the activation energy in kJ·mol^{-1} at constant conversion. Using Equation 5, the activation energy was obtained from a linear slope of plots of log(ϕ) against $1/T_\alpha$ at a constant value of conversion.

2.3.2 Kissinger-Akahira-Sunose (KAS) method

The KAS method is based on the integral isoconversional method where the activation energy is a function of the degree of conversion. KAS consists [18] of extending the Kissinger method into the conversion range 0.1-0.9, and is based on Equation 2 as follows:

$$ln\frac{\phi}{T_\alpha^2} = \ln\frac{AR}{E_a\ g(x)} - \frac{E_a}{RT_\alpha} \tag{6}$$

Plots of $\ln(\phi/T_\alpha^2)$ against $1/T_\alpha$ for a constant value of conversion give a straight line according to Equation 6 whose slope was used to calculate the activation energy of TATB.

2.3.3 Friedman Method

The Friedman method [19] is probably the most general of the differential isoconversional methods and is described by the following relation:

$$\ln(\phi\frac{d\alpha}{dT_\alpha}) = \ln[k\ f(\alpha)] - \frac{E_{a\alpha}}{RT_\alpha} \tag{7}$$

The value of the activation energy for a constant values of conversion was calculated from a linear regression by plotting $\ln[\phi(d\alpha\,|\,dT_\alpha)]$ against $1/T_\alpha$.

2.3.4 Kissinger's method

The activation energy of the main exothermic decomposition reaction is evaluated by applying Kissinger's method [20]. According to Kissinger's equation:

$$ln\frac{\phi}{T_{max}^2} = \ln\frac{AR}{E_a\, g(x)} - \frac{E_a}{RT_{max}} \tag{8}$$

where T_{max} is the peak temperature of the DTG or DTA curves at applied heating rate. The activation energy was calculated from the slope of the straight line by plotting $\ln(\phi/T_{max}^2)$ against $1/T_{max}$.

2.4.5 Reaction models

The reaction models for decomposition were calculated through various Coats and Redfern and Criado methods [21]. Coats and Redfern [22] proposed an integral method by making some approximations which are successfully applied for the prediction of the decomposition reaction mechanism for different solid substances using Equation 9:

$$\ln\frac{g(\alpha)}{T_\alpha^2} = \ln\frac{AR}{qE_a} - \frac{E_a}{RT_\alpha} + \ln\left(1 - \frac{2RT}{E_a}\right) \cong \ln\frac{AR}{qE_a} - \frac{E_a}{RT_\alpha} \tag{9}$$

Here $\ln\dfrac{g(\alpha)}{T_\alpha^2}$, calculated for different solid state reactions with corresponding temperature values at a single heating rate against $1000/T_\alpha$, gives a single master straight line. The activation energy and the pre-exponential factor were calculated from the slope and intercept through ordinary least square estimation combined with different solid reaction models as shown in Table 1.

The reaction models of decomposition were also obtained by the standard Criado method [23, 24]. The $Z(\alpha)$ experimental master plots were obtained by combining the differential and integral forms of the reaction models. According to this method, the reaction models are predicted by applying $Z(\alpha)$ master plots where the activation energy calculated from the isoconversional methods does not significantly change with the extent of conversion. The plots are obtained using Equation 10:

$$Z(\alpha) = f(\alpha)g(\alpha) = \left(\frac{d\alpha}{dt}\right)_t T_\alpha^2 \left[\frac{\pi(x)}{\phi T_\alpha}\right] \tag{10}$$

where $x = \dfrac{E_a}{RT_\alpha}$. Then the activation energy (E_a) is replaced with an average

value of the activation energy (E_o) that is inserted into Equation 10. It is also established that the term in the bracket of Equation 10 has a negligible effect on the shape of the $Z(\alpha)$ function.

Table 1.   Solid-state rate expressions of integral $g(\alpha)$ and differential $f(\alpha)$ for different reaction models of solid state processes

Sr No.	Model	Differential form	Integral form
	Nucleation models		
1	Power law (P$_2$)	$2\alpha^{(1/2)}$	$\alpha^{(1/2)}$
2	Power law (P$_3$)	$3\alpha^{(2/3)}$	$\alpha^{(1/3)}$
3	Power law (P$_4$)	$4\alpha^{(3/4)}$	$\alpha^{(1/4)}$
4	Power law (P$_{2/3}$)	$2/3\ \alpha^{-1/2}$	$\alpha^{3/2}$
5	Avarami-Erofeyev (A$_2$)	$2(1-\alpha)[-\ln(1-\alpha)]^{1/2}$	$[-\ln(1-\alpha)]^{1/2}$
6	Avarami-Erofeyev (A$_3$)	$3(1-\alpha)[-\ln(1-\alpha)]^{2/3}$	$[-\ln(1-\alpha)]^{1/3}$
7	Avarami-Erofeyev (A$_4$)	$4(1-\alpha)[-\ln(1-\alpha)]^{3/4}$	$[-\ln(1-\alpha)]^{1/4}$
	Geometrical contraction models		
8	Contracting area (R$_2$)	$2(1-\alpha)^{1/2}$	$[1-(1-\alpha)^{1/2}]$
9	Contracting volume (R$_3$)	$3(1-\alpha)^{2/3}$	$[1-(1-\alpha)^{1/3}]$
	Diffusion models		
10	1-D Diffusion (D$_1$)	$1/(2\alpha)$	α^2
11	2-D Diffusion (D$_2$)	$[-\ln(1-\alpha)]^{-1}$	$[(1-\alpha)\ln(1-\alpha)] + \alpha$
	Reaction-order models		
12	First-order (F$_1$)	$(1-\alpha)$	$-\ln(1-\alpha)$
13	Second-order (F$_2$)	$(1-\alpha)^2$	$(1-\alpha)^{-1} - 1$

# 3   Results and Discussion

3.1 Physical properties

The particle density of aged and unaged TATB was measured by using a sample of approximately 25 g. The particle density of aged and unaged samples was found to be same within experimental error, namely around 1.913 ±0.002 g·cm^{-3}. The mean particle size was determined using a particle size analyzer (Malvern Mastersizer) and was found to be around 36 μm. The color of aged and unaged TATB was the same, namely yellow-brown crystals. The melting point was measured using DSC under a nitrogen atmosphere. In DSC, the sample was heated through a temperature range of 25-600 °C at a heating rate of 10 °C·min^{-1}. The traces do not show a prominent endothermic peak corresponding to the

melting point (~354 ±0.5 °C), followed by thermal decomposition. According to Ubbelohde, the proximity of the values of the heat of vaporization and the formation of crystal lattice defects contribute to this phenomenon [25].

3.2 Thermal decomposition study by TGA

Figure 1 shows TG and first derivative thermogravimetric (DTG) curves for aged TATB recorded at different heating rates of 5 °C·min^{-1}, 10 °C·min^{-1}, 20 °C·min^{-1}, 30 °C·min^{-1} and 40 °C·min^{-1}. The TG curve did not exhibit any change in mass below 344 °C at a heating rate of 5 °C·min^{-1}. This indicated that it is thermally stable up to a temperature of 344 °C which is almost same value as previously published [15]. The TG curves of aged samples showed that the mass loss occurred in two steps: 85-88% of the mass loss occurred in the first step over the temperature range 344.1-384.1 °C at different heating rates due to degradation of molecular structure, whereas 8-10% of the mass loss occurred in the second step over a wide range of temperature and was completed by about 700 °C. This may be attributed due to loss of decomposition by-products produced in the first step.

Figure 1 also shows DTG curves overlapped within TG curves of TATB. A single peak for thermally decomposition appeared around 362 °C at a heating rate of 5 °C·min^{-1}. It exhibited well-defined initial decomposition temperature (T_{onset}), final decomposition temperature (T_{endset}) and the temperature at the maximum decomposition reaction rate (T_{max}). The thermal data derived from TG/DTG curves are listed in Table 2. It can be seen that T_{onset} and T_{max} values were shifted toward the upper range of temperature with increasing heating rates.
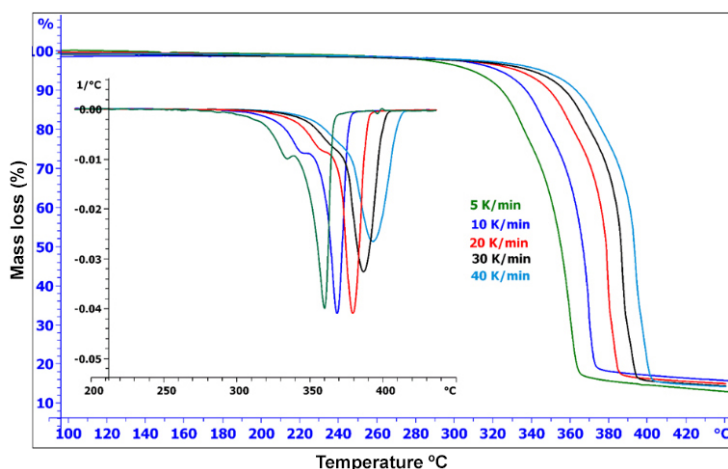

Figure 1. TG/DTG curves for aged TATB obtained at different heating rates under a nitrogen atmosphere

The curves in Figure 2 show the dependence of the conversion with temperature for different heating rates under a nitrogen atmosphere. No remarkable change in the mass loss can be seen up to a temperature of 310 °C after which there is a sudden change in the mass loss in a single step where their slopes increased along with the temperature. Most of the samples were depleted in the temperature range 330-400 °C at the different heating rates studied.

Table 2. Thermal data interpretation in terms of T_{onset}, T_{endset}, and T_{max} of TATB obtained in the temperature range 25-600 °C for different heating rates under a nitrogen atmosphere

Sample	Heating rate [°C·min^{-1}]	Decomposition temperature [°C]		
		T_{onset}	T_{endset}	T_{max}
Aged TATB	5	344.1	362.1	359.0
	10	356.8	373.2	370.8
	20	373.5	385.5	385.2
	30	379.3	393.1	389.2
	40	384.1	401.3	397.8
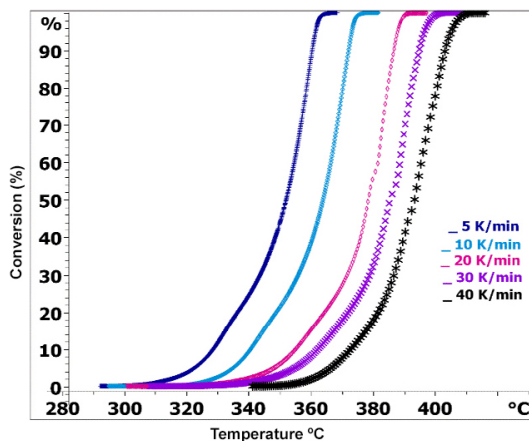
Figure 2. Curves showing the dependence of the conversion against temperature for aged TATB

3.3 Thermal decomposition kinetics

The thermal decomposition kinetics for the first step was performed by means of the isoconversional method using non-isothermal TG at different heating rates. The FWO Equation 5 was employed to determine the activation energies with the extent of conversion. Figure 3 shows FWO plots obtained by plotting $\log(\phi)$

against $1/T_\alpha$ at different conversion. The activation energies calculated from a set of straight lines are listed in Table 3 along with their correlation coefficient constants. The mean activation energy was found to be around 164.9 kJ·mol^{-1} by the FWO method. The squares of the correlation coefficients for linear regression of the activation energy were greater than 0.993. The results show that the activation energy gradually increased up to a conversion of 0.6, followed by a decrease with the extent of conversion.

Table 3. Kinetic parameters of aged TATB for thermal decomposition obtained from the FWO, KAS and Friedman methods
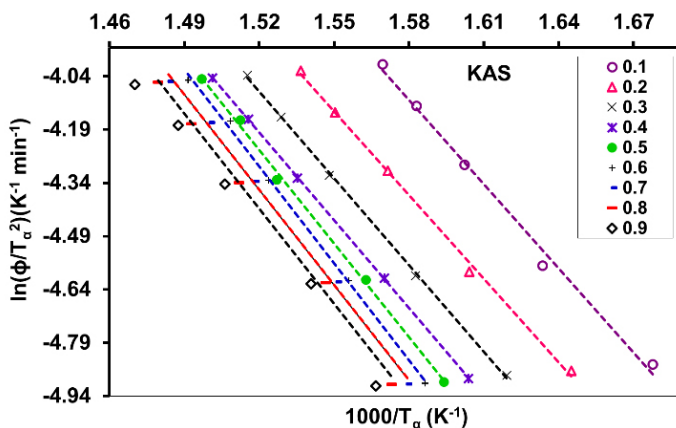
Conversion	FWO		KAS		Friedman	
	E_a [kJ·mol^{-1}]	R^2	E_a [kJ·mol^{-1}]	R^2	E_a [kJ·mol^{-1}]	R^2
0.1	152.5	0.994	150.3	0.997	155.5	0.993
0.2	153.5	0.998	151.3	0.993	156.3	0.998
0.3	158.1	0.999	155.8	0.999	161.0	0.999
0.4	160.0	1	157.7	0.998	163.1	1
0.5	169.2	0.998	168.1	1	172.7	0.998
0.6	175.1	0.998	174.2	0.998	178.7	0.998
0.7	172.3	0.997	171.5	0.997	175.9	0.997
0.8	172.1	0.997	171.1	0.997	174.4	0.997
0.9	171.0	0.996	170.8	0.997	173.1	0.995
Mean	164.9 ±3.4		163.4 ±3.4		167.9 ±3.3	

Note: R^2 is the square of the correlation coefficient for linear regression.
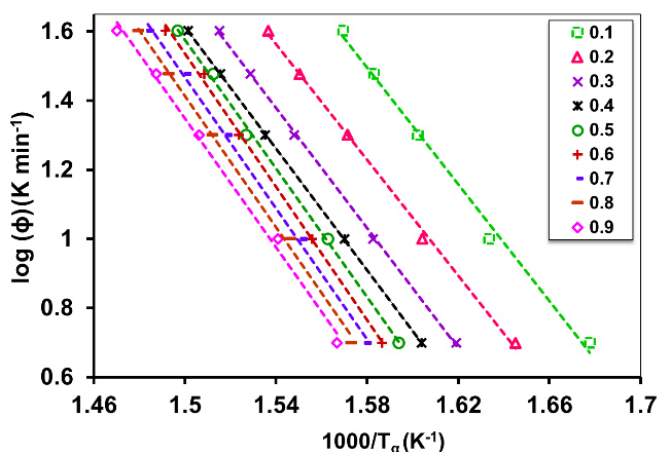
Figure 3. FWO plots of aged TATB at different conversion.

The activation energy was also determined for the first step of decomposition using the KAS Equation 6, which was obtained from the slope of plots of $\ln(\phi/T_\alpha^2)$ against $1000/T_\alpha$ for different extents of conversion. Figure 4 shows KAS plots for extents of conversion in the range 0.1-0.9. The activation energy and the correlation coefficient calculated from the slope are listed in Table 3. The mean activation energy for thermal degradation was found to be around 163.4 kJ·mol^{-1}. It can be seen that the mean activation energy obtained by the KAS method is in good agreement and close to those obtained from FWO method. For accuracy, the more reliable Friedman method was also applied for verifying the above mentioned results as recommended by the International Confederation of Thermal Analysis and Calorimetry (ICTAC) and kinetics committee [26]. The necessary data for graphical representation of $\ln\left(\phi\dfrac{d\alpha}{dT}\right)$ against $(1/T_\alpha)$ were drawn using Equation 7 at the maximum reaction rate.


Figure 4.   KAS plots of aged TATB at different conversion

Figure 5 demonstrates the kinetic analysis by means of the Friedman plots from which the activation energies were calculated. The activation energy obtained from this calculation procedure was a linear slope for all conversions. The activation energies along with the squares of the correlation coefficients are listed in Table 3. The values obtained by this method are close to those obtained using the FWO and KAS methods. Therefore, all methods exhibited the same trend in the activation energies for the overall decomposition reaction for a whole conversion. To verify the kinetic parameters obtained from the isoconversional methods, the kinetic parameters were further investigated by applying the Kissinger model using the temperature at maximum decomposition rate from the DTG data as listed in Table 2. Figure 6 shows Kissinger plots

where $\ln(\phi/T_{max}^2)$ is plotted against $1/T_{max}$ and from where the activation energy was calculated from the linear slope. The overall activation energy for the whole thermal decomposition reaction was obtained and found to be around 179.7 kJ·mol^{-1}. These values are in good agreement and close to the activation energy obtained from the isoconversional methods for conversions of 0.5 or 0.6.
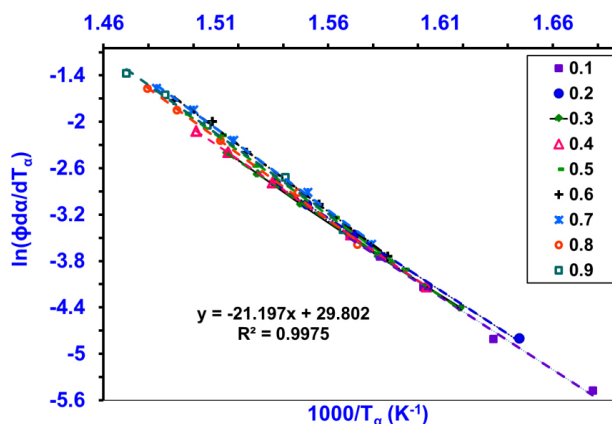
**Figure 5.**   Friedman plots of TATB at different conversion
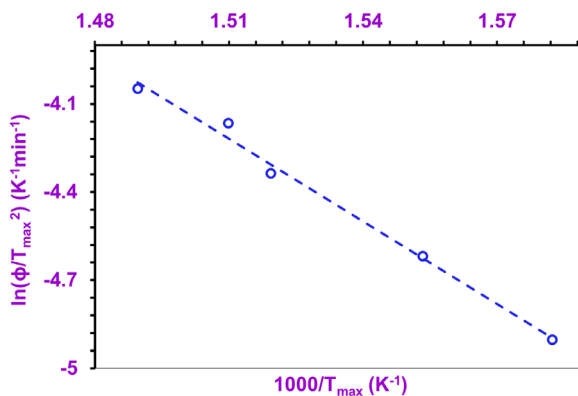
Figure 6.   Kissinger's plots of aged TATB obtained from the temperature at the maximum decomposition reaction rate from DTG data

Table 4. The activation energy and pre-exponential factor of aged and unaged TATB obtained using the Kissinger method on DTG and DTA data

Sample	Method	Kinetic parameters		
		E_a [kJ·mol^{-1}]	A [s^{-1}]	R^2
Aged TATB	DTG	179.7	19.27×10^{13}	0.998
	DTA	176.9	9.89×10^{13}	0.998
Unaged TATB	DTA	178.1	14.89×10^{13}	0.992

In contrast to the mass loss measurements, the thermal decomposition behaviour of unaged TATB was also computed and compared through non-isothermal DTA under the same experimental conditions. DTA analysis of aged and unaged samples was measured in the temperature range 25-600 °C for different heating rates under a nitrogen atmosphere. Figure 7(a, b) shows DTA curves with a single exothermic peak due to the thermal decomposition of TATB. A displacement in the temperature was clearly observed on changing the heating rate because of the delay in transferring heat from the furnace to the sample seen in the temperature of the samples lagging behind that of the furnace temperature at high heating rate. The thermal data for T_{onset}, T_{max}, and T_{endset} for unaged TATB are listed in Table 5. The temperatures at maximum reaction rate (peak) are very close to the thermal data obtained using TG and DTA for aged TATB. This confirms that the thermal stability of TATB does not change due to aging for 20 years under direct contact with the casing and natural environment conditions.
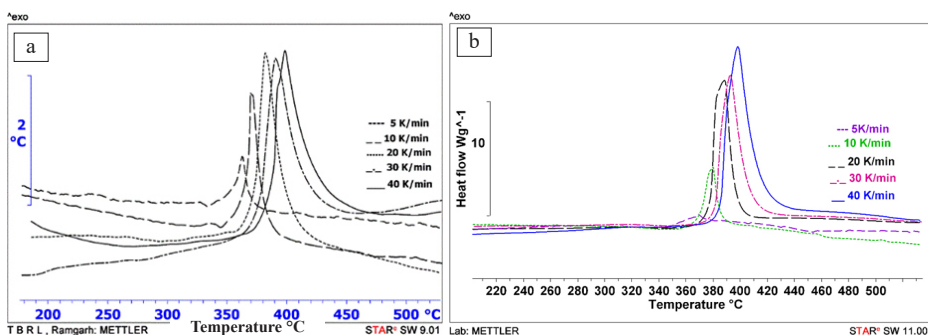
Figure 7. DTA curves of a) aged and b) unaged TATB obtained in the temperature range 25-600 °C at different heating rates under a nitrogen atmosphere

Table 5. The thermal data interpolation in terms of T_{onset}, T_{endset}, and T_{max} of unaged TATB obtained in the temperature range of 25-600 °C for different heating rates under a nitrogen atmosphere

| Heating rate [°C·min^{-1}]	Thermal decomposition [°C]		
	T_{onset}	T_{endset}	T_{max}
5	356.1	370.6	360.2
10	369.8	381.1	373.9
20	377.3	395.9	388.3
30	380.9	406.2	392.7
40	384.6	413.6	399.1
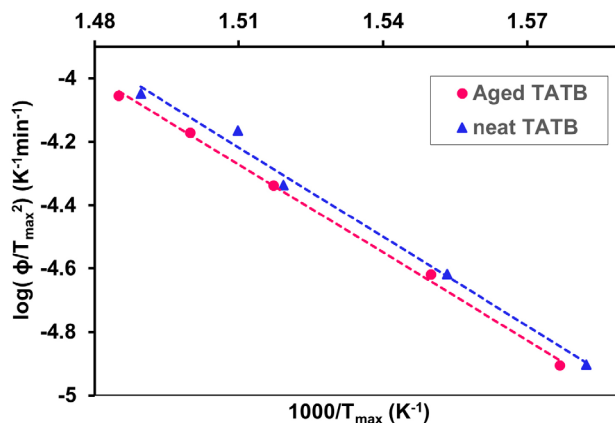
Figure 8. Kissinger's plot of aged (—●—) and unaged (—▲—) TATB using DTA peak temperature at maximum of decomposition reaction rate for different heating rates

To see the effect of aging on TATB, the kinetic parameters obtained using the isoconversional methods were verified through the Kissinger method which is based on the heat flow measurements made using DTA data. This model provides useful information about the activation energy comparable with the activation energy maximum for half conversion in the isoconversional method. This method gives only a single value for the activation energy at the maximum decomposition reaction rate without a knowledge of its actual kinetic complexity. Figure 8 shows Kissinger plots for aged and unaged TATB using DTA fitting data. The activation energy obtained for aged TATB was around 176.9 kJ·mol^{-1}, while the activation energy for the whole decomposition reactions for unaged TATB was around 178.1 kJ·mol^{-1} with pre-exponential factors of 9.89×10^{13} s^{-1} and 14.89×10^{13} s^{-1}, respectively. From the tables we can see that the measured

results are close to that of the KAS methods and the difference between them is small (less than 1%). Linear least squares fits for all kinetic methods by applying temperature peak for maximum reaction rate give good values for the regression coefficients.

3.4 Dependence of activation energy with conversion

Figure 9 shows the dependence for the activation energy of aged TATB with the extent of conversion. The activation energy is initially low and slightly increases up to a certain value of conversion. Then it is suddenly found to increase to a maximum value, followed by a drop with the extent of conversion. It is noticed that there is a significant variation in the activation energy depending on the extent of conversion. In the conversion range 0.1-0.4, the mean activation energy was found to be around 153.8 kJ·mol^{-1}, while for the conversion range 0.5-0.9 this energy reached around 171.1 kJ·mol^{-1}. This difference in the mean activation energy of the two phases is significant during the thermal decomposition. Similar variations in the activation energies for other high explosives have been published in the literature. In this case, it is necessary to use other kinetic methods which can be used to investigate and determine the kinetic parameters and hence separate these processes.
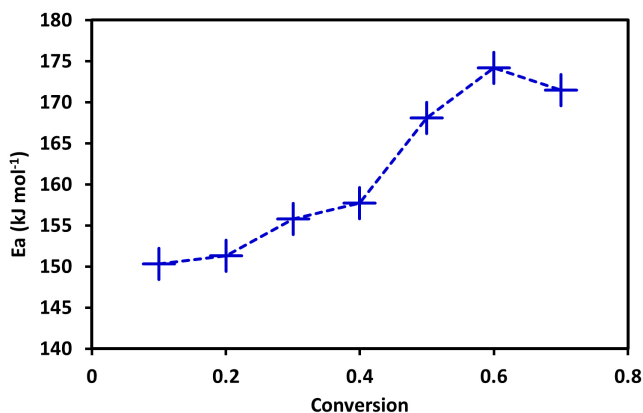
Figure 9. Dependence for the activation energy against extent of conversion for aged TATB obtained using the KAS method

For comparison with the literature, isotopic effects on kinetic measurements were investigated by means of the isothermal DSC method using TATB-H and TATB-D. The entire decomposition progresses as a solid state process within the temperature range 287-382 °C with an activation energy of 247.3 kJ·mol^{-1} [27].

Stolovy *et al.* [28] obtained an activation energy of 258.0 ±16 kJ·mol^{-1} for the first exothermic decomposition reaction. Catalano and Crawford [29] investigated two overlapping exothermic peaks by isothermal DSC over the temperature range 342-357 °C. They reported an activation energy in the range 209-251 kJ·mol^{-1} for the first step and 209-335 kJ·mol^{-1} for the second step. Several theoretical studies have also reported a high activation energy for C−NO$_2$ bond scission mechanisms [30-32]. Chemical kinetic decomposition models have been investigated for multistep chemical species by means of times to thermal explosion for laser ignition experiments [33]. The difference between our results and reported values may be due to differences in particle size, crystal perfection, crystal habit, impurities, method and techniques.

Recently some studies have also suggested that elimination of water may be the predominant channel for thermal decomposition of TATB [30]. The decomposition process was accompanied by stepwise reactions with elimination of water molecules. The primary step involved the formation of an aci-isomer of TATB [33] with a relatively low activation energy of 176.1 kJ·mol^{-1}. It was also established that the heat of vaporization could be characterized by its heat of sublimation of 168.2 kJ·mol^{-1} for the temperature range 129.9-177.3 °C [34]. These values are very close to our result for the activation energy of 167.8 kJ·mol^{-1} as obtained using the Friedman method for aged TATB thermolysis in the temperature range 340-394 °C. In a previous study, the kinetic parameters for TATB bonded with commercially fluoropolymers was studied using isoconversional methods and the activation energy was measured as lying in the range 152.3-170.2 kJ·mol^{-1} [35].

3.5 Reaction mechanisms

Many methods and models have been proposed for solid-state thermal decomposition reactions based on certain mechanistic assumptions. The reaction model was investigated using the Coats-Redfern method to obtain experimental data, and a suitable reaction model was identified by comparing the activation energy which the squares of the correlation coefficient showed was well fitted. Table 1 shows four groups of theoretical reaction models; nucleation and growth models (A_n), geometrical contraction models (R_n), diffusion models (D_n) and reaction-order models (F_n).

Table 6 shows the results for the activation energies and squares of the correlation coefficients for linear regression obtained from fitting $\ln[g(\alpha)/T_\alpha^2]$ against $1000/T_\alpha$ for a heating rate of 10 °C·min^{-1}. It can be seen that the correlation coefficients for nucleation and growth, and the reaction order models do not fit the experimental data well. The power law and diffusion models are

the best fits as their correlation coefficients for linear regression are greater than 0.990, but their activation energies do not match the experimental activation energies. On the other hand, the activation energies obtained using the Coats-Redfern method for geometrical contraction models (R_2 and R_3) are in good agreement with those obtained using isoconversional methods with the squares of the correlation coefficients greater than 0.990. Therefore the reaction model could probably best be described by geometrical contraction reaction mechanisms.

Table 6. Kinetic parameters for thermal decomposition of aged TATB calculated from the Coats-Redfern method for solid-state reaction mechanisms

Model	Kinetic parameters		R^2
	E_a [kJ·mol^{-1}]	A [s^{-1}]	
P_2	231.4	1.2×10^5	0.995
P_3	70.1	2.7×10^5	0.995
P_4	43.3	2.0×10^6	0.994
$P_{2/3}$	96.4	1.4×10^{18}	0.996
A_2	88.8	9.8×10^5	0.983
A_3	39.3	5.4×10^6	0.984
A_4	55.8	2.2×10^7	0.978
D_1	310.9	5.0×10^{24}	0.996
D_2	333.2	2.4×10^{26}	0.994
D_3	357.6	9.4×10^{27}	0.990
R_2	168.2	7.7×10^{12}	0.992
R_3	174.5	1.8×10^{13}	0.990
F_1	187.9	8.0×10^{14}	0.984

The reaction mechanism was further verified by using the more reliable Criado method as recommended by ICTAC and its thermal committee [26]. This method was used for calculating experimental master plots using Equation 10. These plots are directly calculated from the experimental data by subtracting the activation energy obtained using the Kissinger method and a heating rate of 10 °C·min^{-1}. Theoretical master plots were also obtained by combining the differential and integral forms of the solid-state reaction models using Equation 10 as listed in Table 1. A suitable reaction model was identified by comparing the experimental and theoretical master plots (Figure 10). In the theoretical approach, most of the master plots initially increased up to a certain value of conversion, followed by a decrease with extent of conversion, while some plots are represented by a straight line. In the experimental approach, the master plot

somehow overlapped with the theoretical contraction reaction model master plot. Therefore, the reaction model may be probably described by the contraction reaction mechanisms.
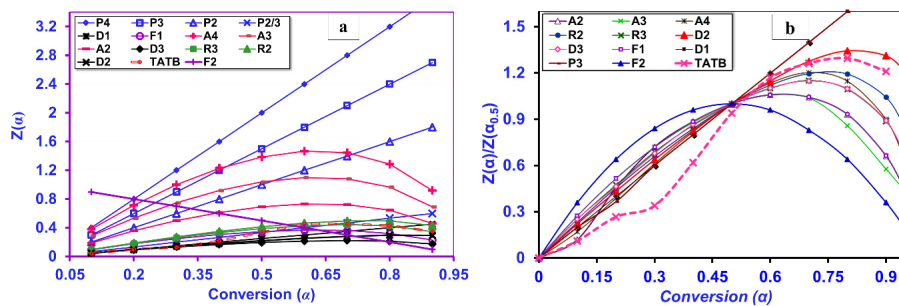
Figure 10. The theoretical and experimental master $Z(\alpha)$ plots for reaction models of solid-state processes; a) the master plots for $Z(\alpha)$ against conversion, b) $Z(\alpha)/Z(\alpha_{0.5})$ against conversion at heating rate of 10 °C·min^{-1} using activation energy obtained by KAS method

For better understanding, using a reference at point $\alpha = 0.5$ and according to Equation 10, the following Equation 11 is derived;

$$\frac{Z(\alpha)}{Z(\alpha_{0.5})} = \frac{f(\alpha)g(\alpha)}{f(\alpha_{0.5})g(\alpha_{0.5})} = \frac{\left(\frac{d\alpha}{dt}\right)_t T_\alpha^2 \left[\frac{\pi(x)}{\phi T_\alpha}\right]}{\left(\frac{d\alpha_{0.5}}{dt}\right)_{t_{0.5}} T_{0.5}^2 T_{0.5}^2 \left[\frac{\pi(x_{0.5})}{\phi T_{0.5}}\right]} \tag{11}$$

where $x_{0.5} = E_o/RT_{0.5}$; $T_{0.5}$ and $t_{0.5}$ are the temperature and time required to attain 50% conversion, respectively. Using Equation 11, Figure 10b shows theoretical and experimental master plots with extent of conversion for aged TATB. This plot probably best agreed with the contraction reaction model after a conversion of 0.4. Below a conversion of 0.4, the master plot does not exactly overlap with any theoretical master plots, indicating that the decomposition process is not described by a single reaction model. These results support recent theoretical studies published in the literature [36]. Our findings suggest that this type of material could probably best be described by multi-phase or parallel thermal decomposition reactions.

3.6 FTIR studies

Figure 11 shows an FTIR spectrum of the aged TATB. The bands at 3315 cm^{-1} and 3213 cm^{-1} are characteristic of the asymmetrical and symmetrical N−H stretching vibrations respectively. The two bands at 1561 cm^{-1} and 1220 cm^{-1} can be attributed to the corresponding asymmetrical and symmetrical N−O stretching vibrations respectively. Meanwhile, the bands at 1602 cm^{-1} and 729 cm^{-1} may be ascribed of the C−N stretching of the amino groups. The bands at 1442 cm^{-1} and 1173 cm^{-1} are assigned to the skeletal stretching modes of the aromatic ring. The spectrum shows that there is no measurable change in the position of absorption bands and new bands formation in this chemical structure. The results are in good agreement with that of commercially pure TATB [37, 38].
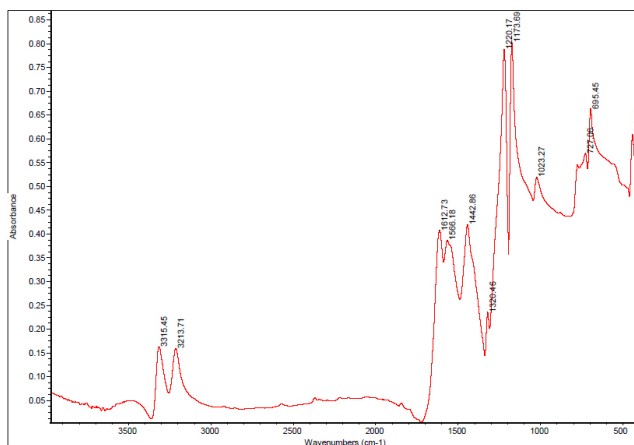
Figure 11. FTIR spectrum of aged TATB

3.7 SEM studies

Figures 12a and 12b show SEM micrographs of aged and unaged TATB. It can be seen that the particles for unaged TATB are of irregular shape and separated from each other. Small micropores can be seen on the surface of the sample. Figure 12b shows a similar type of micrograph for the aged sample. This indicates that the surface morphology does not change with aging under natural environmental conditions for a time period of 20 years.
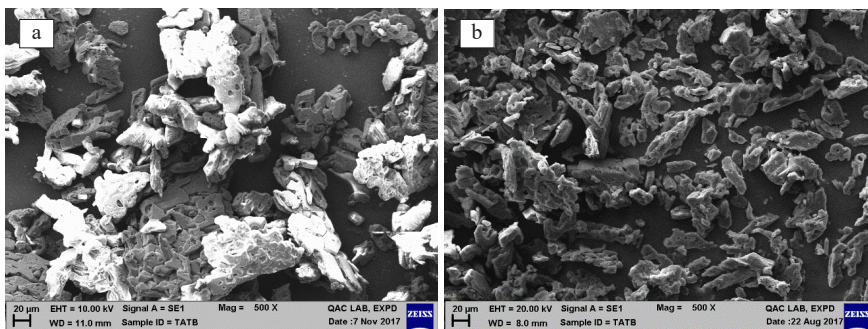
Figure 12. SEM micrographs of a) unaged and b) aged TATB

3.8 Thermodynamic parameters

After the kinetic parameters had been obtained using various kinetic methods, the thermodynamic parameters such as change of enthalpy $\Delta H^{\#}$, Gibbs free energy $\Delta G^{\#}$, and entropy $\Delta S^{\#}$ for formation of the activated complex [39] were calculated using the following equations [12-14]. These parameters are important indicators of thermal safety.

$$A \cdot exp\frac{-E}{RT} = \nu \cdot \exp\frac{-\Delta G^{\#}}{RT} \tag{12}$$

$$\Delta H^{\#} = E - RT \tag{13}$$

$$\Delta G^{\#} = \Delta H^{\#} - T\Delta S^{\#} \tag{14}$$

where $\Delta G^{\#}$, $\Delta H^{\#}$ and $\Delta S^{\#}$ are the Gibbs free energy, enthalpy and entropy of the activation, $\nu = \frac{K_B}{h}T$; K_B is the Boltzmann's constant ($1.38 \cdot 10^{-23}$ J·s^{-1}); h is the Planck constant ($6.626 \cdot 10^{-34}$ J·s^{-1}). The parameters $\Delta G^{\#}$, $\Delta H^{\#}$ and $\Delta S^{\#}$ were computed at different heating rates by means of the temperature at maximum decomposition reaction rate using Equations 12-14. The results for $\Delta G^{\#}$, $\Delta H^{\#}$ and $\Delta S^{\#}$ are presented in Table 7. The physical meaning of $\Delta H^{\#}$ is the energy that the molecules absorb to change from the common state to the activated state; thus the value of $\Delta H^{\#}$ is much closer to that of the activation energy. $\Delta G^{\#}$ is the chemical potential for activation course. The positive values of $\Delta H^{\#}$ and $\Delta G^{\#}$ show that they are connected with the introduction of heat which is a non-spontaneous process with stable state in normal conditions. These parameters are consistent with the kinetic parameters.

Table 7. Thermodynamic parameters for thermal decomposition of aged
           TATB obtained at different heating rates under a nitrogen atmosphere

Sample	Heating rate [°C·min^{-1}]	T_{max} [K]	$\Delta G^{\#}$ [kJ·mol^{-1}]	$\Delta H^{\#}$ [kJ·mol^{-1}]	$\Delta S^{\#}$ [J·mol^{-1}·K^{-1}]
Aged TATB	5	632.0	166.7	156.7	−15.8
	10	643.8	166.8	156.6	−15.8
	20	658.2	166.9	156.5	−15.8
	30	662.2	166.9	156.5	−15.8
	40	670.8	167.0	156.4	−15.8
			166.68 ±0.03	156.54 ±0.03	−15.8

3.9 Critical and self-accelerating decomposition temperatures

The characteristic temperatures for thermal decomposition such as the peak
temperature at maximum reaction rate, (T_{max}), the critical temperature of thermal
explosion (T_b), and the self-accelerating decomposition temperature (T_{SADT}) are
important indicators of the thermal safety. T_b and T_{SADT} were determined from
the DTA data using the following equations [40];

$$T_{max0} = T_{max} - (a\phi + b\phi^2 + c\phi^3) \tag{15}$$

$$T_b = \frac{E_a - \sqrt{E_a^2 - 4E_a RT_{max^o}}}{2R} \tag{16}$$

$$T_{SADT} = T_b - \frac{RT_b^2}{E_a} \tag{17}$$

where a, b and c are fitting constants, R is the gas constant, and E_a is the activation
energy obtained using the Kissinger method. Finally, T_b and T_{SADT} for aged TATB
were found to be 357.0 °C and 338.3 °C, respectively. These temperature values
are low compared to the temperature at the maximum reaction rate. However,
this does not mean that TATB suffers from safety problems. Thus we conclude
that these values lie within the acceptable limit and safe range for processing,
handling, storage and use.

4   Conclusions

This paper has reported the effect of aging on the properties of a 20 year old TATB that has been in direct contact with a casing under natural environment conditions. No significant changes in characteristic properties such as surface morphology, chemical and thermal properties have been found for the aged TATB. TG/DTA data along with all the calculation methods employed for the kinetic parameters are close to those found in the published literature. The kinetic parameters were investigated using the isoconversional methods and compared with the Kissinger method based on the peak temperature at maximum reaction rate. The reaction models were studied using the Coats-Redfern and Criado methods. The activation energies are in good agreement with those obtained from the Coats-Redfern method for geometrical contraction models where data is best fitted for linear regression. The results of the Criado method further support the thermal decomposition reaction models obtained from the Coats-Redfern method. The reaction models studied by the Criado method indicate that decomposition reactions are accompanied by multi-step reaction mechanisms. The surface morphology and thermal properties of aged TATB do not show significant changes under natural aging for a prolonged period of time. The critical temperatures for thermal explosion, *i.e.* T_b and T_{SADT}, were around 357.0 °C and 338.3 °C respectively. Our findings show that the values for $\Delta G^{\#}$, activation enthalpies ($\Delta H^{\#}$) and activation entropies ($\Delta S^{\#}$) are around 166.68 ±0.03 kJ·mol^{-1}, 156.54 ±0.03 kJ·mol^{-1} and −15.8 J·mol^{-1}·K^{-1}, respectively. Based on the collected data, the storage life for TATB can be easily computed for its use in civilian and military service.

References

[1] Rice, S. F.; Simpson, R. L. *The Unusual Stability of TATB: A Review of the Scientific Literature*. Lawrence Livermore National Laboratory, Livermore, CA, Report UCRL-LR-103683, **1990**.

[2] Dobratz, B. M. *The Insensitive High Explosive Triaminotrinitrobenzene (TATB):*

     Development and Characterization − 1888 to 1994. Report LA-13014-H, Los
     Alamos Scientific Laboratory, NM, Los Alamos **1995**.

[3] Voreck, W. E.; Brooks, J. E.; Eberhardt, J. R.; Rezaie, H. A. *Shaped Charge for
     a Perforating Gun Having a Main Body of Explosive Including TATB and a Sensitive
     Primer*. Patent US 5597974, **1997**.

[4] Nouguez, B.; Mahe, B.; Vignaud, P. O. Cast PBX Related Technologies for IM
     Shells and Warheads. *Sci. Technol. Energ. Mater.* **2009**, *70*: 135-139.

[5] Borman, S. Advanced Energetic Materials Emerge for Military and Space
     Applications. *J. Chem. Eng. News* **1994**, *72(3)*: 18-22.

[6] Adler, J. Thermal Explosion Theory with Arrhenius Kinetics: Media. *Proc. R. Soc.
     London A* **1991**, 329-335.

[7] Ajadi, S. O.; Nave, O. Approximate Critical Conditions in Thermal Explosion
     Theory for a Two-Steps Kinetic Model. *J. Math. Chem.* **2010**, *47*: 790-807.

[8] Weifeia, Y.; Tonglaia, Z.; Junb, Z.; Yigangb, H.; Gangb, L.; Chaob, H.; Jinshanb, L.;
     Huib, H. Effect of Microwave Irradiation on TATB Explosive (II): Temperature
     Response and other Risk. *J. Hazard. Mater*. **2010**, *173*: 249-252.

[9] Foltz, M. F.; Ornellas, D. L.; Pagoria, P. F.; Mitchell, A. R. Recrystallization and
     Solubility of 1,3,5-Triamino-2,4,6-Trinitrobenzene in Dimethyl Sulfoxide. *J. Mater.
     Sci.* **1996**, *31*: 1893-1901.

[10] Britt, A. D.; Moniz, W. B.; Chingas, G. C.; Moore, D. W.; Heller, C. A.; Ko, C. L.
     Free Radicals of TATB. *Propellants Explos. Pyrotech.* **1981**, *6*: 94-95.

[11] Manaa, M. R.; Schmidt, R. D.; Overturf, G. E.; Watkins, B. E.; Fried, L. E.;
     Kolb, J. R. Towards Unraveling the Photochemistry of TATB. *Thermochim. Acta*
     2002, *384*: 85-90.

[12] Hoffman, D. M.; Matthews, F. M.; Pruneda, C. O. Dynamic Mechanical and
     Thermal Analysis of Crystallinity Development in Kel-F 800 and TATB/Kel-F
     800 Plastic Bonded Explosives. Part I. Kel-F 800. *Thermochim. Acta* **1989**, *156*:
     365-72.

[13] Singh, A.; Soni, P. K.; Singh, M.; Srivastava, A. Thermal Degradation, Kinetics
     and Correlation Models of Poly(Vinylidene Fluoride-Chlorotrifluoroethylene)
     Copolymers. *Thermochim. Acta* **2012**, *548*: 88-92.

[14] Singh, A.; Soni, P. K.; Shekharam, T.; Srivastava, A. A Study On Thermal Behaviour
     of a Poly(VDF-CTFE) Copolymers Binder for High Energy Materials. *J. Appl.
     Polym. Sci.* **2013**, *127*(3): 1751-1757.

[15] Singh, A.; Sharma, T. C.; Kumar, M.; Narang, J. K.; Kishore, P.; Srivastava, A.
     Thermal Decomposition and Kinetics of Plastic Bonded Explosives Based
     on Mixture of HMX and TATB with Polymer Matrices. *Def. Tech.* **2016**; doi.
     org/10.1016/j.dt.2016.11.005.

[16] Flynn, J. H.; Wall, L. A General Treatment of the Thermogravimetry of Polymers.
     J. Res. Natl. Bur. Std. A Phys. Chem. **1966**, *70*: 487-523.

[17] Ozawa, T. A New Method of Analyzing Thermogravimetric Data. *Bull. Chem.
     Soc. Jpn*. **1965**, *38*: 1881-1886.

[18] Akahira, T.; Sunose, T. Method of Determining Activation Deterioration Constant

of Electrical Insulating Materials. *Res. Report Chiba Inst. Technol. (Sci. Technol.)* **1971**, *16*: 22-31.

[19] Kissinger, H. E. Reaction Kinetics in Differential. *J. Therm. Anal. Chem.* **1957**, *29*: 1702-1706.

[20] Friedman, H. Kinetics of Thermal Degradation of Char-Forming Plastics from Thermogravimetry: Application to a Phenolic Plastic. *J. Polym. Sci. Part C* **1964**, *6*: 183-195.

[21] Criado, J. M.; Perez-Maqueda, L. A.; Gotor-Malek, F. J. J.; Koga, N A Unified Theory for the Kinetic Analysis of Solid State Reactions under any Thermal Pathway. *J. Therm. Anal. Calorim.* **2003**, *72*: 901-906.

[22] Coats, A. W.; Redfern, J. P. Kinetic Parameters from Thermogravimetric Data. *Nature (London)* **1964**, *201*: 68-69.

[23] Perez-Maqueda, L. A.; Criado, J. M.; Gotor, F. J.; Malek, J. Advantages of Combined Kinetic Analysis of Experimental Data Obtained Under any Heating Profile. *J. Phys. Chem. A* **2002**; *106*: 2862-2868.

[24] Paterson, W. L. Computation of the Exponential Trap Population Integral of Glow Curve Theory. *J. Comput. Phys.* **1971**, *7*(1): 187-190.

[25] Zeman, S. The Thermoanalytical Study of Some Aminoderivatives of 1,3,5-Trinitrobenzene. *Thermochim. Acta* **1993**, *216*: 157-168.

[26] Vyazovkin, S.; Burnham, A. K.; Criado, J. M.; Perez-Maqueda, L. A.; Popescu, C.; Sbirrazzuoli, N. ICTAC Kinetics Committee Recommendations for Performing Kinetic Computations on Thermal Analysis Data. *Thermochim. Acta* **2011**, *520*: 1-19.

[27] Rogers, R. N.; Janney, J. L.; Ebinger, M. H. Kinetic-Isotope Effects in Thermal Explosions. *Thermochim. Acta* **1982**, *59*: 287-298.

[28] Stolovy, A.; Jones, E. C.; Aviles, J. B.; Namenson, A. I.; Fraser, W. A. Exothermic Reactions in TATB Initiated by an Electron Beam. *J. Chem. Phys.* **1983**, *78*: 229.

[29] Catalano, E.; Crawford, P. C. An Enthalpic Study of the Thermal Decomposition of Unconfined Triaminotrinitrobenzene. *Thermochem. Acta* **1983**, *61*: 23-36.

[30] Wu, C. J.; Fried, L. E. Ring Closure Mediated by Intramolecular Hydrogen Transfer in the Decomposition of a Push-Pull Nitroaromatic: TATB. *J. Phys. Chem. A* **2000**, *104*: 6447-6452.

[31] Shao, J.; Cheng, X.; Yang, X. The CNO_2 Bond Dissociation Energies of Some Nitroaromatic Compounds: DFT Study. *Struct. Chem.* **2006**, *17*: 547-550.

[32] Manaa, M. R.; Fried, L. E. The Reactivity of Energetic Materials under High Pressure and Temperature. In: *Energetic Materials* (Sabin, J. R., Ed.) Academic Press, Cambridge MA, USA **2014**.

[33] Tarver, C. M. Chemical Kinetic Modeling of HMX and TATB Laser Ignition Tests. *J. Energ. Mat.* **2004**, *22*: 93-104.

[34] Rosen, J. M.; Dickinson, C. Vapor Pressures and Heats of Sublimation of Some High Melting Organic Explosives. *J. Chem. Eng. Data* **1969**, *14*: 120-24.

[35] Singh, A.; Sharma, T. C.; Kishore, P. Thermal Degradation Kinetics and Reaction Models of 1,3,5-Triamino-2,4,6-trinitrobenzene-based Plastic-bonded Explosives

Containing Fluoropolymer Matrices. *J. Therm. Anal. Calorim.* **2017**, *129*: 1403-14.

[36] Tsyshevsky, R. V.; Sharia, O.; Kuklja, M. M. Molecular Theory of Detonation Initiation: Insight from First Principles Modelling of the Decomposition Mechanisms of Organic Nitro Energetic Materials. *Molecules* **2016**, *21*: 236.

[37] Xu, H.; Duan, X.; Li, H.; Pei, C. A. A Novel High-Energetic and Good-sensitive Co-crystal Composed of CL-20 and TATB by a Rapid Solvent/Non-Solvent Method. *RSC Adv.* **2015**, *5*: 95764-95770.

[38] Huang, B.; Minhua Cao, M.; Wu, X.; Nie, F.; Huang, H.; Hu, C. Twinned TATB Nanobelts: Synthesis, Characterization, and Formation Mechanism. *Cryst. Eng. Comm.* **2011**, *13*: 6658-6664.

[39] Tompa, A. S.; Boswell, R. F. Thermal Stability of a Plastic Bonded Explosive. *Thermochim. Acta* **2000**, *357-358*: 169-75.

[40] Zhang, T. L.; Hu, R. Z.; Xie, Y.; Li, F. P. The Estimation of Critical Temperatures of Thermal Explosion for Energetic Materials Using Non-isothermal DSC. *Thermochim. Acta* **1994**, *244*: 17.